Design, Fabrication, and Preliminary Testing of Air-Bearing Test Vehicles for the Study of Autonomous Satellite Maneuvers

S. Kwok-Choon, K. Buchala, B. Blackwell, S. Lopresti, M. Wilde, T. Go

Florida Institute of Technology
150 West University Boulevard
Melbourne, Florida, 32901

skwokcho2006@my.fit.edu, kbuchala2011@my.fit.edu, blackwellb2010@my.fit.edu, stuart@lopresti.org, mwilde@fit.edu, tgo@fit.edu

ABSTRACT

This paper explores the design, fabrication, and preliminary testing of two air-bearing vehicles to serve as the core of a satellite maneuvering testbed. The two air-bearing vehicles are a platform for the development and testing of formation flight, autonomous docking and capture control systems, different types of capture mechanisms, relative navigation sensors, and on-orbit servicing verification experiments.

The air-bearing vehicles produce a thin film of nitrogen between microporous carbon air-bearings and a 1.8 m by 3.6 m glass plate on top of a vibration-insulated optical bench, resulting in virtually frictionless planar motion. Systems testing on an air-bearing table is a cost-effective method for experimental validation of guidance, navigation, and control systems. The air-bearing vehicles are equipped with cameras, Microsoft Kinect sensors, accelerometers, an eight-thruster reaction control system, a reaction wheel, and various grippers and grasping features. The motion of the two vehicles is continuously tracked by an OptiTrack motion capture system, permitting a wide range of autonomous and tele-operated control approaches.

With a focus on the lessons learned during the design, fabrication, integration, and testing of the air-bearing test vehicles. Preliminary testing explored open loop control to perform linear, and rotation maneuvers. Outlined are the main steps required to build this pair of air-bearing test vehicles. First, the design and parts fabrication. Second, the assembly and testing of subsystems. Third, a discussion of the communication relay with a series of dynamic experiments, that allowed for calculation of the average force and associated error exerted from each solenoid thruster if operating at full capacity.

Keywords

Robotics, Air-Bearing Vehicles, Air-Bearing Table Testing, Preliminary Open Loop Testing, Thruster Force Estimation Method

1. INTRODUCTION

The observation, recognition, and capture of malfunctioning satellites and orbital debris is a growing concern [1,4,6–8,10,13]. Linked to this is the study of different methods to enable rendezvous and capture for small satellite swarming, space debris removal, as well as on-orbit servicing [3,5,9]. NORAD is tracking the orbital debris in Low Earth and Geo-Synchronous Orbit (see Figure 1)

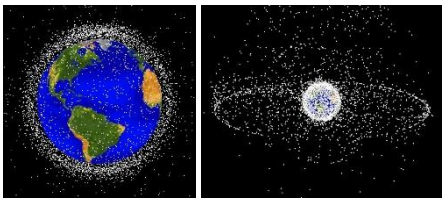

Figure 1: Orbital Debris in Leo [15] and Geo. [16]

Ground testing is a cost effective solution that allows for simulation and testing of simulated satellites, satellite capture methods, rendezvous and docking with uncooperative targets. Various research groups and entities have built ground test facilities in order to verify and refine different experiments and controllers [2,11,12,14]. The air-bearing vehicles described were developed as a platform for the testing of formation flight, autonomous docking and capture control systems, relative navigation sensors, and capture mechanisms.

The paper first describes the design and fabrication of the air-bearing vehicles. It then provides an overview of the communication relay developed to relay commands between the vehicles and control station using User Datagram Protocol (UDP) over Wi-Fi and Ethernet. The tests and main assembly were done at the Orbital Robotic Interaction, On-orbit servicing, and Navigation (ORION) laboratory at Florida Institute of Technology. The results section, describes the open loop translation and rotation tests performed and the preliminary calculation of the Force exerted by the on board thrusters and the associated error based on measurements taken.

2. DESIGN AND FABRICATION

2.1. Design

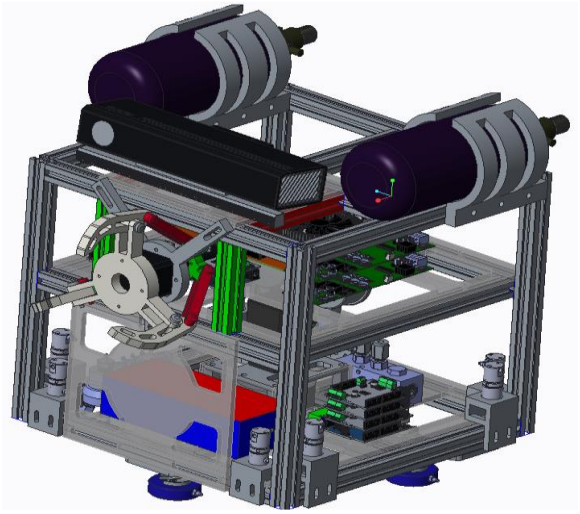

Figure 2: CAD Design

The air-bearing vehicles (ABVs) are designed with the intent of studying planar satellite capture and docking (See Figure 2) are modular; therefore, future improvements are possible based on the test and experimental requirements.

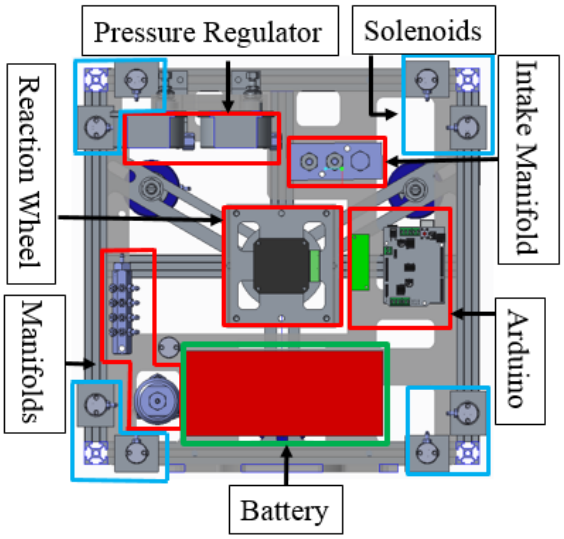

Figure 3: Air Bearing and Pneumatic Systems

The ABVs move on a flat floor with three degrees of freedom (DOF) : translation in the horizontal XY-plane with rotation about the vertical Z-axis. This was possible by using air-bearing pads for floatation, compressed-nitrogen thrusters and an onboard reaction wheel (See Figure 3 and Figure 4). Both the chaser and target ABV have the same propulsion system. Each solenoid provided thrust by actuating open and allowing compressed-nitrogen air to pass through. Initial testing did not use the on board reaction wheel in conjunction with the solenoids.

Located on the upper deck: is the onboard computer, voltage regulators, and the air-bearing chaser vehicle is equipped with a rapid-prototyped three-fingered grasping mechanism with a Kinect V2 sensor system (See in Figure 5). One of the eventual goals is to have a Kinect V2 sensor system installed on board the chaser vehicle used for on-board distance and object recognition with image processing.

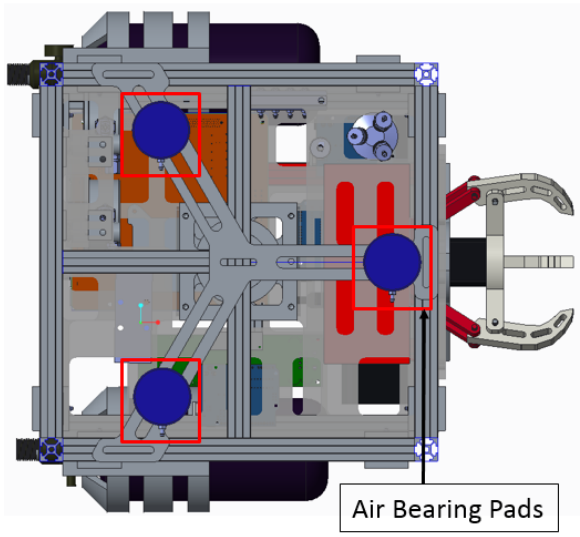

Figure 4: Air Bearing Pads

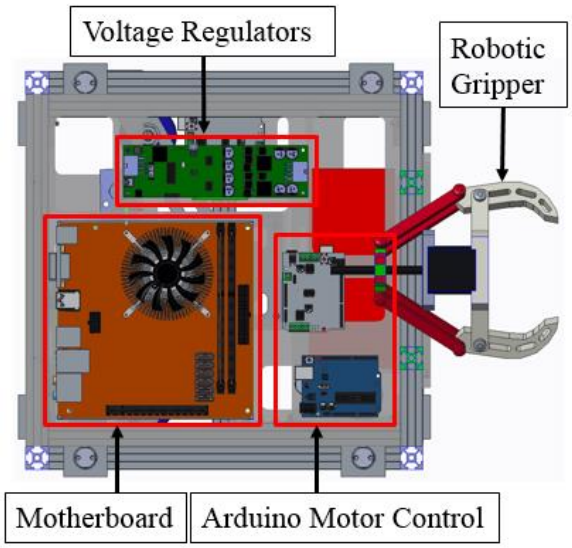

Figure 5: Upper Deck Design

2.2. Fabrication

First the frame was assembled, with the lower layer installed. This included the laser cut acrylic mount surfaces as well as the pressure regulator and pneumatic systems (see Figure 6, 7). With the completion of the CAD and frame design, Fabrication and assembly of the air-bearing vehicles commenced.

Manifold A connected to the air-bearing pads located in the base, with manifold B splitting the air to the solenoids (see Figure 7).

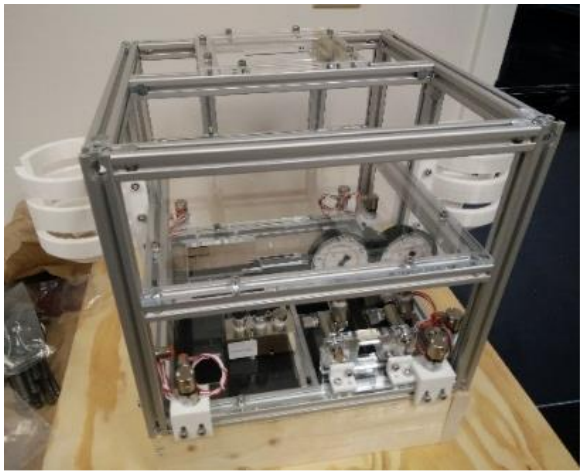

Figure 6: Frame Construction and Pneumatic system

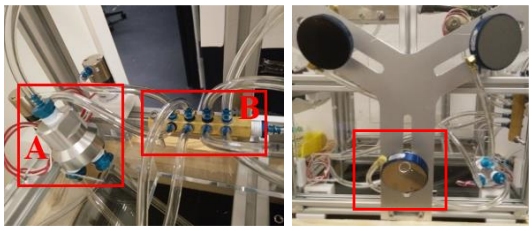

Figure 7: Pressure Manifolds and Air Bearing Pads

The upper deck components (computer, voltage regulators, and microcontrollers) installed and tested after the pneumatic sub-systems (See Figure 5,Figure 8).

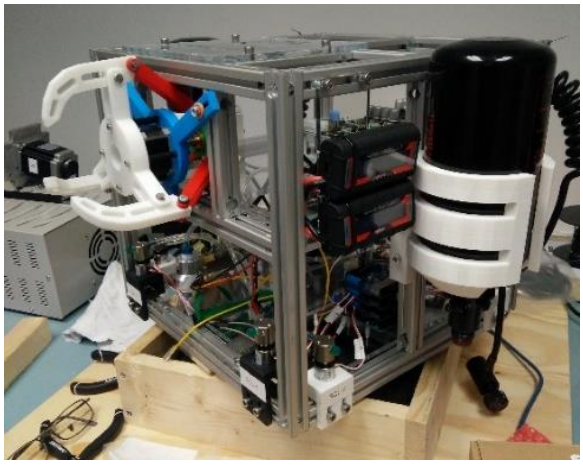

Figure 8: Install Power Regulators: Initial Installation of voltage regulators and wattmeter.

The full assembly of both the chaser and target vehicles shown in Figure 9. In order to help reduce mass. The air tanks' location changed from the sides to on top of the vehicles, with a bumper installed at the base in order to protect the electronic components and reduce the possibility of damage caused by inadvertent collision. The completed chaser and target vehicles are shown (see Figure 9), where the chaser (Right) will now be called Bob, and the target vehicle (Left) called Charlie.

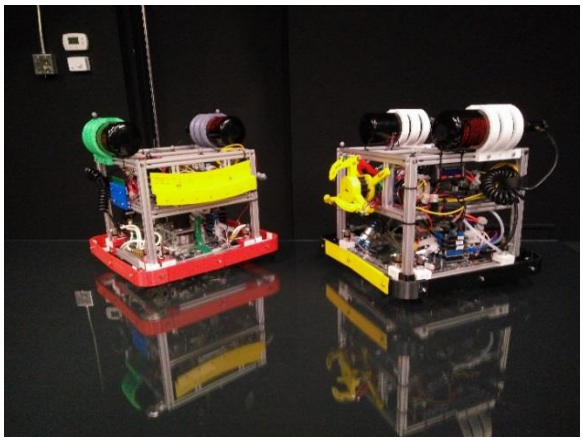

Figure 9: Vehicles fully assembled. Chaser (Bob Right) Target (Charlie Left)

3. COMMUNICATION RELAY

The communication relay infrastructure necessary to send and receive commands between the ABVs and the remote PC control station is illustrated in Figure 10.

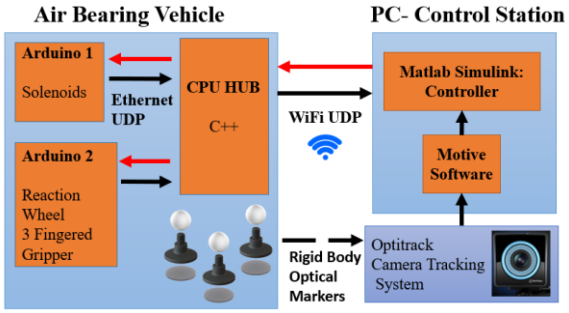

Figure 10: Communication Relay Infrastructure

There are four main segments integrated to work in-sync with one another: Wi-Fi UDP communication between Arduino IDE, C++ HUB on the vehicle using UDP sockets, Matlab Simulink, and Optitrack Motive Software. The communication relay infrastructure provides flexibility and modular growth based on the type of experiment and sensors used.

The major functions of each segment of the communication relay are described in the following sections.

3.1. PC Control Station

The Optitrack Camera System records the global relative position and orientation of the air-bearing vehicle. Motive Software obtains the current position of the defined rigid bodies from the Optitrack Camera System. Matlab Simulink receives and records the broadcasted information over UDP Multicast from the Motive Software. After receiving the broadcasted Optitrack position information, the Matlab-Simulink Controller then sends the control signal to the air-bearing vehicle.

3.2. Air-Bearing Vehicle:

The onboard CPU receives the command from the PC Control Station. With both Arduino 1 and 2 are in communication with the CPU Hub with Ethernet UDP. The CPU sends the appropriate command to the different on board microcontroller. Arduino 1 controls the solenoids used for vehicle planar thruster maneuvering. Arduino 2 controls the gripper as well as the on-board reaction wheel.

4. TESTING SET UP

The ORION laboratory is located at Florida Institute of Technology. The Air-Bearing table with vibration damping is shown at the North side of the ORION Lab near the experiment preparation room (see Figure 11).

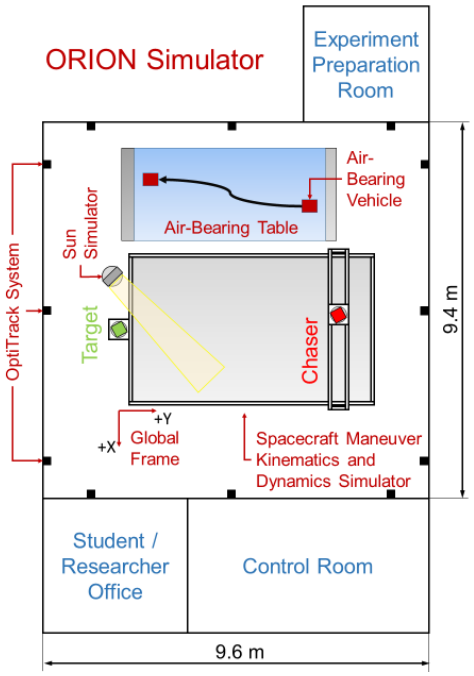

Figure 11: ORION Lab Space

4.1. Test Facility / Test Apparatus

The ORION laboratory features an Optitrack Prime 17W optical tracking system [17,18] that is able to provide position information. The external sensors are used in conjunction, thereby providing real-time system positional awareness, enabling the study of planar orbital object maneuvers between the chaser and target systems.

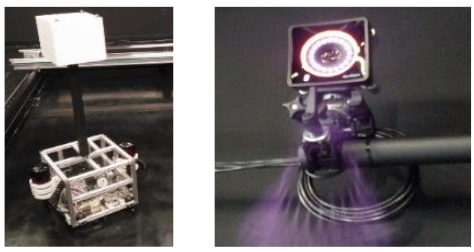

Figure 12: Leak Test (left) and Optitrack Camera (right)

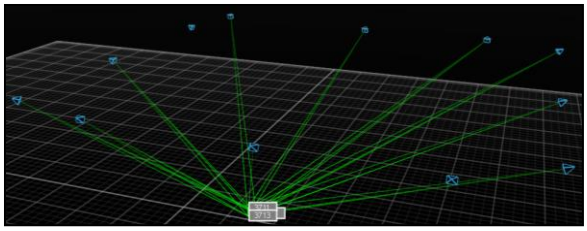

Figure 13: Optitrack Camera Array

The left image of Figure 12 is one of the ABVs at the leak check and pneumatic systems phase done to ensure that there were no air leaks. The right image of Figure 12 shows one of the Optitrack cameras used to track assigned objects (see Figure 12). After initial calibration and 3-dimensional mapping, rigid body objects are defined using Optitrack markers as (see Figure 13). The local body frame of the vehicle shown in Figure 14. The Optitrack system, once set up, is able to track an object as a rigid body, where the [X, Y, Z] are with respect to the global relative frame, and the [θ, ψ, ϕ] angles are with respect to the global coordinate axis frame.

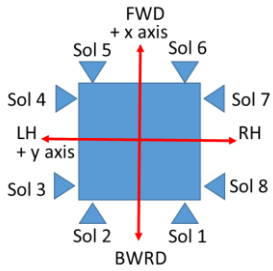

Figure 14: Local Body Frame of the Air-Bearing Vehicle

5. RESULTS

5.1. Open Loop Control: Translation Test

5.1.1. Translation Description of Solenoid Firing

The first series of tests performed was to calculate the force exerted from the solenoid thrusters during an open-loop maneuver as well as the associated error from the measurements recorded. Each air-bearing vehicle has eight solenoid thrusters located around its body (see Figure 15). In order to perform a linear translation maneuver in the +x-axis direction and measure the exerted force on the vehicle. Solenoids 1 and 2 were commanded open with the other solenoids kept in the off position.

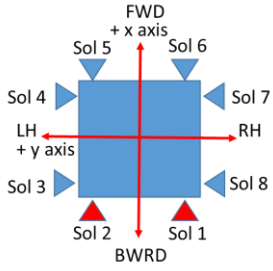

Figure 15: Solenoids turned on for Translation

5.1.2. Air-Bearing Translation Example

The time stamped images of the air-bearing vehicle displayed below (see Figure 16) show the translation command given versus

the distance travelled with time. Possible sources of error for the linear translation experiment include:

1) The solenoids on the vehicle may have been misaligned and not parallel to the x-axis on the body frame
2) The vehicle may not have been exactly level leading to a mass bias on one side of the vehicle versus the other
3) The amount of thrust produced by each thruster may have not been identical.

Figure 16 shows the time-lapse progression of the vehicle as it moves from one side of the air-bearing table to other side from the start to end of a particular run of the experiment.

Figure 16: Translation Example

5.1.3. PWM Solenoid Command

A Pulse Width Modulated (PWM) signal of 100% duty cycle was sent to solenoids 1 and 2, with all other solenoids not engaged. The signal sent to the on-board CPU commanded Sol1 and Sol2 were commanded to be open from 2 seconds to 17 seconds (see Figure 17, Figure 18) with all other solenoids not activated.

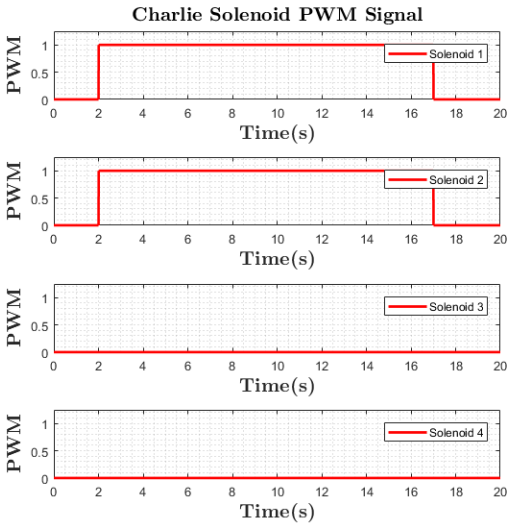

Figure 17: PWM signal Solenoid 1234

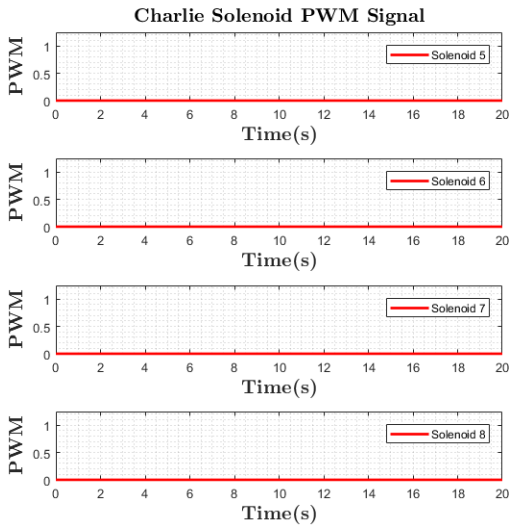

Figure 18: PWM signal Solenoid 5678

5.1.4. Translation Data Collection

Five experimental runs performed to compare the thrust provided versus time and command sent (see Figure 19). Charlie was released from the same relative position in the Global Coordinate Frame of the laboratory. As the vehicle travelled across the optical table, the position was logged for further analysis. The translation of the vehicles X, Y, and θ position shown in Figure 19. There appears to be a larger translation in the Y direction with a relatively small amount of drift in the X direction, and θ heading.

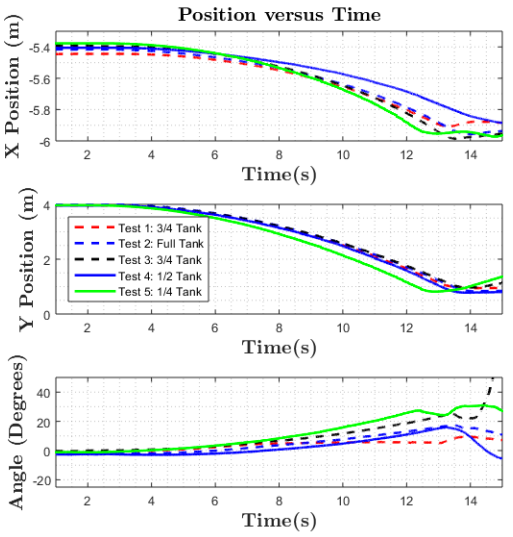

Figure 19: Optitrack Position Tracking of Test Vehicle

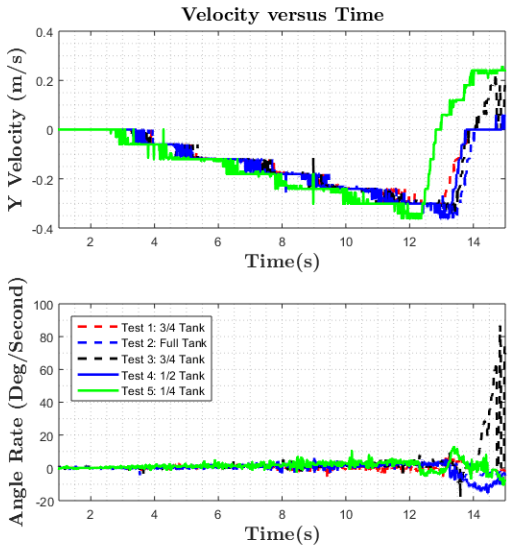

Figure 20: Optitrack Velocity Tracking of Test Vehicle

Figure 20 shows the Optitrack $\dot{Y}, \dot{\theta}$ velocity tracking data for the air-bearing test vehicle. The vehicle is caught at the end of the table is shown when $\dot{Y}$ velocity changes direction at the 12 second mark. During normal operation, AVB is not expected to move at a very fast rate (>5 m/s) across the glass plate surface. Therefore, the current position and filtered velocity data of the rigid body can be used in the future development of a closed loop controller within Matlab-Simulink.

5.1.5. Example data collected from Test 1

This section discusses example data collected during a single experiment run

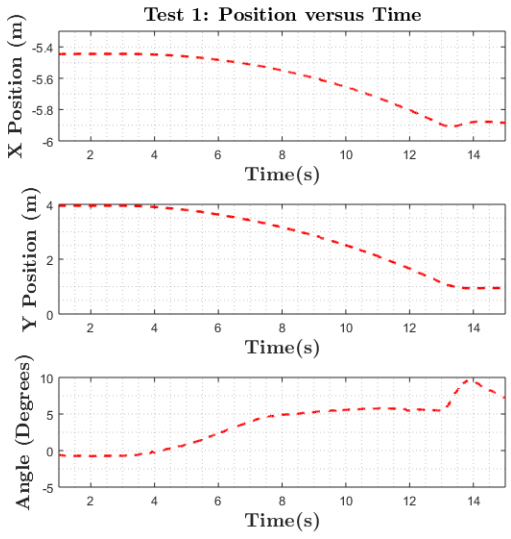

Figure 21: Optitrack Position Tracking Test 1

Figure 21 shows the change in X, Y, and angle θ of the vehicle as it was released from its start position and the linear translation maneuver was performed.

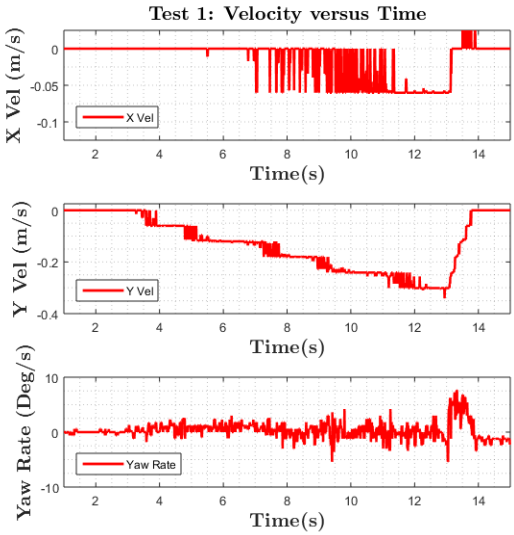

Figure 22: Optitrack Velocity Tracking Test 1

Figure 22 shows the rates of change $\dot{X}, \dot{Y}, \dot{\theta}$ of the vehicle. The point of capture can be seen where the vehicle is stopped, approximately at 12 seconds where the $\dot{Y}$ rate changes direction, to prevent the vehicle from falling off the air-bearing table.

5.1.6. Calculations to determine average force exerted by each thruster during translation

To perform calculations to find the approximate force from the thrusters on the air-bearing vehicle, the boundary conditions outlined in

Table ***1*** apply, with the mass and time measurements in Table 2. The initial velocity of the ABV is zero with the friction forces from the glass surface considered negligible. Error calculations done using Root Mean Square (RMS) approach.

Table 1: Boundary conditions for calculations

$Velocity_{initial}$	$U_i = 0\ m/s$
$Time_{initial}$	$T_i = 2.0\ seconds$
$Time_{final}$	$T_f = 10.0\ seconds$
$Time_{difference}$	$\Delta T = 8.0\ seconds$
Friction Effects	Considered Negligible

Table 2: Mass and Time Measurements

M_A = mass Charlie with no tanks	12.050 kg ± 0.050 kg
M_B = mass of 1 tank full	1.447 kg ± 0.001 kg
M_C = mass of 1 tank empty :	1.364 kg ± 0.001 kg
$M_\Delta = M_B - M_C$ (Mass difference of full versus empty.)	0.083 kg ± 0.001 kg
Ratio of tank1, tank2 filled	R_1, R_2
Measurement error in time, $\frac{\partial \Delta T}{\partial \varepsilon}$	$\pm 0.005\ seconds$
Distance error in the x-direction and y-direction.	$\frac{\partial \Delta x}{\partial \varepsilon}, \frac{\partial \Delta y}{\partial \varepsilon} = \pm 0.5mm$

Calculation for mass of the air-bearing vehicle M_{tot}, was defined as the mass of the tank changes based on the fuel consumed.

$$M_{tot} = M_A + 2M_C + (R_1 + R_2)M_\Delta \quad (1)$$

The mass measurement error was defined:

$$\frac{\partial M_{tot}}{\partial \varepsilon} = \sqrt{\left(\frac{\partial M_{tot}}{\partial M_A}\frac{\partial M_A}{\partial \varepsilon}\right)^2 + \left(\frac{\partial M_{tot}}{\partial M_C}\frac{\partial M_C}{\partial \varepsilon}\right)^2 + \left(\frac{\partial M_{tot}}{\partial M_\Delta}\frac{\partial M_\Delta}{\partial \varepsilon}\right)^2} \quad (2)$$

When performing the series of experiments, the observation was that one test consumed approximately ¼ of the total air capacity of the on board air-tanks, an illustration shown (see Figure 23). One full tank of air had a pressure of 2600 psi. There are two air tanks located on each air-bearing vehicle. An approach to consider is that the mass of the air tanks would vary with time as the propellant was consumed to provide thrust. However to get an approximate of the force provided by the thrusters, the initial mass at the start of each test was considered.

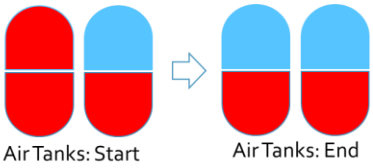

Figure 23: Illustration for Air Tank capacity.

The distance travelled for the air-bearing vehicle,ΔS, with the error in x-direction$\frac{\partial \Delta S}{\partial x}$, and y-direction, $\frac{\partial \Delta S}{\partial y}$:

$$\Delta S = \sqrt{(x_f - x_i)^2 + (y_f - y_i)^2} = \sqrt{(\Delta x)^2 + (\Delta y)^2} \quad (3)$$

With the error in x and y distance expressed respectively as:

$$\frac{\partial \Delta S}{\partial x} = \frac{1}{2}(\Delta x^2 + \Delta y^2)^{-\frac{1}{2}}(2\Delta x) \quad (4)$$

$$\frac{\partial \Delta S}{\partial y} = \frac{1}{2}(\Delta x^2 + \Delta y^2)^{-\frac{1}{2}}(2\Delta y) \quad (5)$$

The full expression for the error in displacement is expressed as:

$$\frac{\partial \Delta S}{\partial \varepsilon} = \sqrt{\left(\frac{\partial \Delta S}{\partial \Delta x}\frac{\partial \Delta x}{\partial \varepsilon}\right)^2 + \left(\frac{\partial \Delta S}{\partial \Delta y}\frac{\partial \Delta y}{\partial \varepsilon}\right)^2} \quad (6)$$

Using the kinematic motion equation:

$$\Delta S = U_i \Delta T + \frac{1}{2}a\Delta T^2$$

After rearranging the acceleration of the vehicle, a, is found:

$$a = \frac{2 * \Delta S}{\Delta T^2}$$

With the error in acceleration of the vehicle:

$$\frac{\partial a}{\partial \varepsilon} = \sqrt{\left(\frac{\partial a}{\partial \Delta S}\frac{\partial \Delta S}{\partial \varepsilon}\right)^2 + \left(\frac{\partial a}{\partial \Delta T}\frac{\partial \Delta T}{\partial \varepsilon}\right)^2} = \sqrt{\left(\frac{2}{\Delta T^2}\frac{\partial \Delta S}{\partial \varepsilon}\right)^2 + \left(\frac{-4\Delta S}{\Delta T^3}\frac{\partial \Delta T}{\partial \varepsilon}\right)^2} \quad (7)$$

With the equation for Force and Force measurement error defined:

$$F = M_{tot}a,$$

$$\frac{\partial F}{\partial \varepsilon} = \sqrt{\left(\frac{\partial F}{\partial M_{tot}}\frac{\partial M_{tot}}{\partial \varepsilon}\right)^2 + \left(\frac{\partial F}{\partial a}\frac{\partial a}{\partial \varepsilon}\right)^2} = \sqrt{\left(a\frac{\partial M_{tot}}{\partial \varepsilon}\right)^2 + \left(M_{tot}\frac{\partial a}{\partial \varepsilon}\right)^2} \quad (8)$$

The amount of air in the tank with the initial and final position listed in

Table 3. The calculated acceleration and mass approximations listed in Table 4. The calculated force exerted by both solenoids as well as the force exerted by one thruster are shown in Table 5.

Table 3: Test Condition, Initial and Final Recorded Position

Test	Air in the tanks at start	$[X \quad Y]_{initial}$ (m)	$[X \quad Y]_{final}$ (m)
1	$\frac{3}{4}$ tanks full	[-5.444 3.953]	[-5.656 2.506]
2	$\frac{4}{4}$ tanks full	[-5.416 3.988]	[-5.638 2.562]
3	$\frac{3}{4}$ tanks full	[-5.393 3.958]	[-5.645 2.581]
4	$\frac{1}{2}$ tanks full	[-5.405 3.957]	[-5.573 2.484]
5	$\frac{1}{4}$ tanks full	[-5.377 3.968]	[-5.671 2.14]

Table 4: Calculated Acceleration and Mass Approximation

Test	$[\ddot{X} \quad \ddot{Y}]$ (m/s^2)	Mass Approximation.
1	[-0.0066 -0.0452]	14.903 kg ± 0.0501kg
2	[-0.0069 -0.0446]	14.944 kg ± 0.0501kg
3	[-0.0079 -0.0430]	14.903 kg ± 0.0501kg
4	[-0.0053 -0.0460]	14.861 kg ± 0.0500kg
5	[-0.0092 -0.0571]	14.820 kg ± 0.0500kg

Table 5: Calculated Force Exerted by Solenoid Thrust

Test	$Force_{12}$ Force exerted by both thrusters	$Force_1$ Force exerted by one thruster
1	0.6811 N ± 0.0025N	0.3405 N ± 0.0025N
2	0.674 N ± 0.0024N	0.3370 N ± 0.0024N
3	0.6519 N ± 0.0017N	0.3260 N ± 0.0017N
4	0.6885 N ± 0.0025N	0.3443 N ± 0.0025N
5	0.8574 N ± 0.0031N	0.4287 N ± 0.0031N

From Table 5, the average force exerted by each of the solenoids on the ABV during the linear translation maneuver can be denoted using the following equation expression:

$$Avg\ F_1 = \frac{\left(\sum_{i=1}^{n=5} F_1(i)\right)}{n} \pm \max\frac{\partial F_1(i)}{\partial \varepsilon} error \quad (9)$$

$$Avg\ F_1 = 0.3553\ N \pm 0.0031\ N$$

5.2. Rotation Test

5.2.1. Rotation Description of Thruster Firing

An open loop command for counter clockwise rotation was performed as a validation experiment to demonstrate that rotation is possible by using solenoids 1,3,5,7 in conjunction with each other. An illustration of which solenoids were commanded to activate can be seen Figure 24.

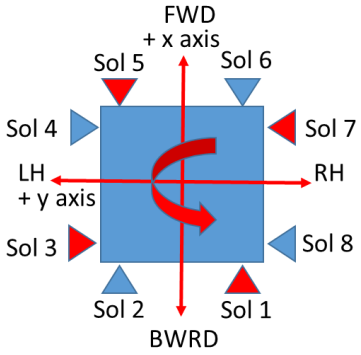

Figure 24: Illustration of Solenoids Turned on for Rotation

The time stamped images obtained from a video recording show the vehicle perform a counter clockwise rotation sequence that was commanded (see Figure 25).

Figure 25: Rotation Command Example

5.2.2. PWM Solenoid Command

The rotation experiment was performed using a PWM duty cycle signal of 80% (see Figure 26 and Figure 27). Where Solenoid Thrusters: Sol1, Sol3, Sol5, Sol7 were commanded to pulse with Sol2, Sol4, Sol6, Sol8 not activated.

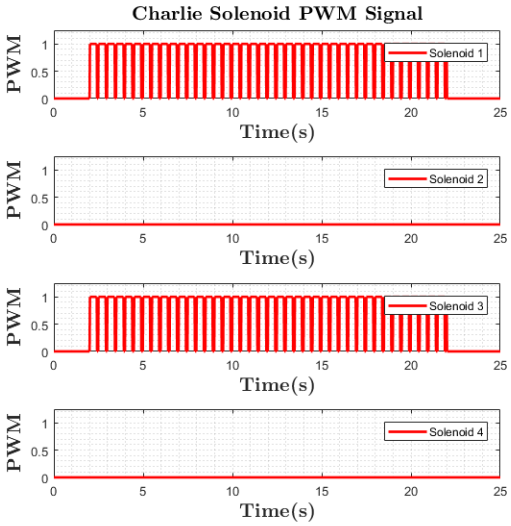

Figure 26: PWM Signal Solenoid 1-2-3-4

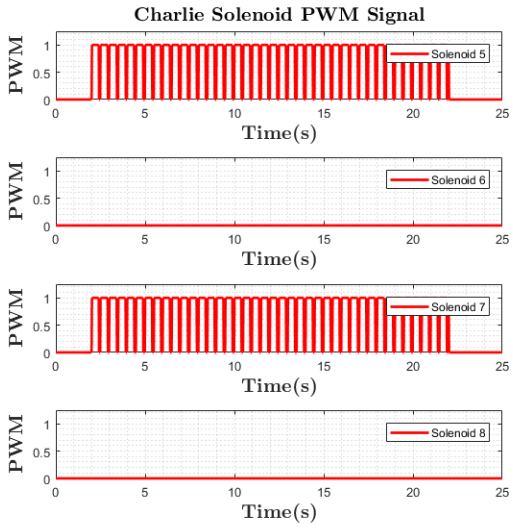

Figure 27: PWM Signal Solenoid 5-6-7-8

5.2.3. Data Collected from Rotation Experiment

The Optitrack system recorded the translation and rotation information of the air-bearing vehicle as shown in the below figure (see Figure 28). The data shows the rotation of the vehicle being tracked by Optitrack in the angle θ, as well as the global position X and Y. There does appear to be some noise in the signal recorded by Optitrack, this is shown in the fluctuation of the angle, θ, data.

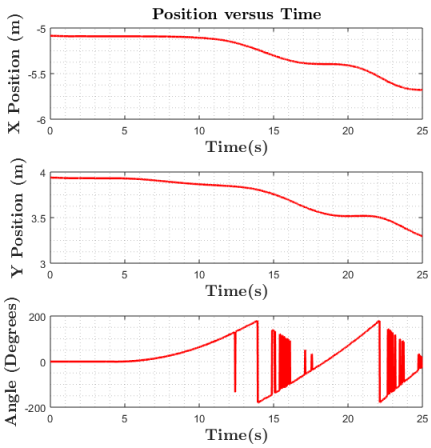

Figure 28: Rotation Position Tracking

6. CONCLUSION

Covered is the design, fabrication, and communication relay created for the ABVs. The first series of experiments included open loop command to perform linear translation and a rotation experiments. Calculations were made to gain an estimation for the thrust exerted from each solenoid. In conclusion, the main objectives of preliminary testing were met; however, future work includes the creation of a closed loop controller in order to perform trajectory and position control in 3-DOF. With the additional testing of both the chaser and target air-bearing vehicles together in order to achieve rendezvous and docking.

The model and theory equations are extendable to the 3D motions. However, to have the capability of orbital 6-DOF motion would require a re-design and following a similar path to the SPHERES program for MIT that performs testing on the ISS station or parabolic flight experiments. While possible, undertaking such a task would present its own set of technical and logistic complexities.

7. ACKNOWLEDGEMENTS

Acknowledgements include Stuart LoPresti with assistance in the fabrication, assembly, and testing process of the air-bearing vehicle. Kendrick Buchala and Branden Blackwell for assistance with experimental testing and vehicle tracking. As well as assistance provided by the Florida Tech Makerspace, Machine Shop, and MAE faculty.

8. REFERENCES

[1] F Aghili. 2008. Optimal control for robotic capturing and passivation of a tumbling satellite with unknown dynamics. *AIAA Guid. Navig. Control Conf.* August (2008). Retrieved from http://arc.aiaa.org/doi/pdf/10.2514/6.2008-7274

[2] Farhad Aghili and Kourosh Parsa. 2008. An adaptive vision system for guidance of a robotic manipulator to capture a tumbling satellite with unknown dynamics. *2008 IEEE/RSJ Int. Conf. Intell. Robot. Syst. IROS* (2008), 3064–3071. DOI:https://doi.org/10.1109/IROS.2008.4650758

[3] Angel Flores-Abad and Ou Ma. 2012. Control of a space robot for minimal attitude disturbance to the base satellite for capturing a tumbling satellite. *SPIE Defense, Secur. Sens.* 8385, (2012), 83850J–83850J–12. DOI:https://doi.org/10.1117/12.918523

[4] Marshall H Kaplan and D Ph. 2009. Survey of Space Debris Reduction Methods. September (2009), 1–11.

[5] Shuichi Matsumoto, Steven Dubowsky, Stephen Jacobsen, and Yoshiaki Ohkami. 2003. Fly-By Approach and Guidance for Uncontrolled Rotating Satelite Capture. August (2003), 5745.

[6] Shin-Ichiro Nishida, Satomi Kawamoto, Yasushi Okawa, Fuyuto Terui, and Shoji Kitamura. 2009. Space debris removal system using a small satellite. *Acta Astronaut.* 65, (2009), 95–102. DOI:https://doi.org/10.1016/j.actaastro.2009.01.041

[7] Shin Ichiro Nishida and Satomi Kawamoto. 2011. Strategy for capturing of a tumbling space debris. *Acta Astronaut.* 68, 1–2 (2011), 113–120. DOI:https://doi.org/10.1016/j.actaastro.2010.06.045

[8] Carmen Pardini and Luciano Anselmo. 2014. Acta Astronautica Review of past on-orbit collisions among cataloged objects and examination of the catastrophic fragmentation concept $. *Acta Astronaut.* 100, (2014), 30–39. DOI:https://doi.org/10.1016/j.actaastro.2014.03.013

[9] Ary Pizarro-Chong and Arun K. Misra. 2008. Dynamics of multi-tethered satellite formations containing a parent body. *Acta Astronaut.* 63, (2008), 1188–1202. DOI:https://doi.org/10.1016/j.actaastro.2008.06.021

[10] Richard Rembala, Frank Teti, and Patrice Couzin. 2012. Operations concept for the robotic capture of large orbital debris. *Adv. Astronaut. Sci.* 144, (2012), 111–120.

[11] Marco Sabatini, Giovanni B Palmerini, and Paolo Gasbarri. 2015. Acta Astronautica A testbed for visual based navigation and control during space rendezvous operations $. *Acta Astronaut.* 117, (2015), 184–196. DOI:https://doi.org/10.1016/j.actaastro.2015.07.026

[12] Jana L Schwartz and Christopher D Hall. 2003. Historical Review of Air-Bearing Spacecraft Simulators Introduction. 26, 4 (2003). DOI:https://doi.org/10.2514/2.5085

[13] G. Tommei, a. Milani, and a. Rossi. 2007. Orbit determination of space debris: Admissible regions. *Celest. Mech. Dyn. Astron.* 97, (2007), 289–304. DOI:https://doi.org/10.1007/s10569-007-9065-x

[14] Wenfu Xu, Bin Liang, and Yangsheng Xu. 2011. Acta Astronautica Survey of modeling , planning , and ground verification of space robotic systems. *Acta Astronaut.* 68, 11–12 (2011), 1629–1649. DOI:https://doi.org/10.1016/j.actaastro.2010.12.004

[15] leo640.jpg (JPEG Image, 640 × 640 pixels). Retrieved April 12, 2018 from https://www.orbitaldebris.jsc.nasa.gov/images/beehives/leo640.jpg

[16] geo640.jpg (JPEG Image, 640 × 512 pixels). Retrieved April 12, 2018 from https://www.orbitaldebris.jsc.nasa.gov/images/beehives/geo640.jpg

[17] OptiTrack - Motion Capture Systems. Retrieved April 11, 2018 from https://optitrack.com/

[18] OptiTrack - Prime 17W - Wide angle coverage for large volumes in smaller spaces. Retrieved April 11, 2018 from https://optitrack.com/products/prime-17w/